Macromolecules

Article

pubs.acs.org/Macromolecules

Microscopic Study of Chain Deformation and Orientation in Uniaxially Strained Polymer Networks: NMR Results versus Different Network Models

Maria Ott,*[,†] Roberto Pérez-Aparicio,[‡] Horst Schneider,[†] Paul Sotta,[‡] and Kay Saalwächter*[,†]

[†]Institut für Physik − NMR, Martin-Luther-Universität Halle-Wittenberg, Betty-Heimann-Str. 7, 06120 Halle, Germany

[‡]Laboratoire Polymères et Matériaux Avancés, UMR 5268, CNRS/Rhodia-Solvay, 85 avenue des Frères Perret, F-69192 Saint Fons, France

Supporting Information

ABSTRACT: The complex pathway of transmitted stress and strain within elastic networks affects the conformations of single network chains in a complex and inhomogeneous manner. For a novel experimental assessment, we investigated moderately to highly cross-linked vulcanized natural rubber networks with proton multiple-quantum NMR and studied the correlation between macroscopic uniaxial elongation and local effects of strain and/or confinement on the level of elastically active subchains. Our method and the data treatment allow for a separate analysis of chain deformation and orientation, which in turn allows for critical comparisons of our experimental results with predictions from various network models. Specifically, comparisons with the affine fixed-junction model, the phantom model, and different tube models allowed us to draw conclusions on the presence of possibly tube-related local confinement effects. As none of the models alone was able to provide a comprehensive, quantitative description of all experimental data, we performed numerical calculations inspired by earlier simulation results, which match the data and support the presence of two distinct populations of network chains that are either more or less stretched as well as oriented.

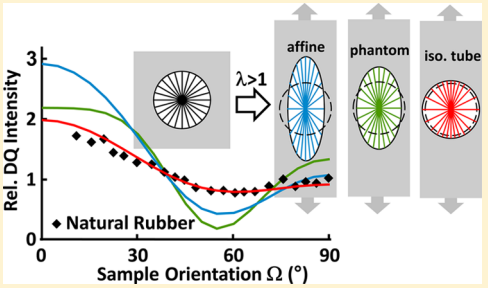

I. INTRODUCTION

Elastomers exhibit outstanding mechanical properties as they do not only sustain very high elongations without rupture but also return to their original state with no or little residual deformation. At the microscopic level, these unique properties result from a complex interplay between chemically and/or physically connected network chains. However, available statistical models to describe the elasticity on the molecular level still fail to quantitatively describe the local response of the systems as well as their macroscopic properties.[1−8] One of the reasons may be the lack of experimental methods sensitive enough to reveal the complexity of the local network structure characterized by the diverse configurations of the individual network chains and by the presence of defects.[9] If available, such microscopic knowledge could be used to improve theory.

Currently, two major experimental approaches delivering information about the local structure of polymer networks stand out, i.e., neutron scattering and NMR techniques. In particular, small-angle neutron scattering (SANS) is sensitive to the *static intrachain pair correlation function* of individual polymer chains[10] and accesses the instantaneous ensemble average of the radius of gyration of labeled chains in the network, usually retrieved in parallel and perpendicular to the stretching direction.[1] In various NMR techniques, among them the ^{1}H multiple-quantum (MQ) NMR experiments used herein, the local deformation and orientation of the network chains are probed via an *orientational time averaging* of the dipole−dipole interaction tensors of protons in chain segments that belong to a spatially constrained local subchain.[11] The technique thus reports on the magnitude of local segmental orientation correlations as imposed by the cross-links/constraints and, if present, the macroscopic deformation. The intrinsic millisecond time scale of such NMR experiments allows the subchains to sample their full conformational space relevant for the macroscopic entropic elasticity and thus to test near-equilibrium properties, provided that the systems are probed at high enough temperature above T_g.[8,11] The NMR observable as measured on undeformed elastomers is thus directly proportional to their elasticity modulus.[8,12,13] The only related technique, probing the constraints to segmental translations, is neutron spin echo (NSE) spectroscopy, which was previously used to corroborate the validity of a specific tube model,[14] yet the dynamic structure factor as its main observable has a less direct relation to the macroscopic properties of the sample.

SANS measurements and their analyses are not straightforward, as easily interpretable data on elastically active chain deformation are restricted to end-linked polymer networks[1] or

Received: June 19, 2014
Revised: October 13, 2014
Published: October 28, 2014

   dx.doi.org/10.1021/ma5012655 | Macromolecules 2014, 47, 7597−7611

require the variation of the length of a labeled path in networks made by peroxide cross-linking of long chains,[15] in order to reach the relevant local and potentially subaffine length scales. Problems may arise from the potentially high defect chain fractions of such systems[15−18] and the lack of possibilities to uniquely remove or take into account defect contributions.[9] The noteworthy features and advantages of the ^{1}H MQ NMR technique are that no labeling of the chains is necessary, that the spatial resolution is fixed to the well-defined length scale of the local cross-link/constraint density, and that the nonelastic defect content is probed directly and can easily be taken into account.[17,18] Moreover, the technique provides the opportunity to derive not only an ensemble average value for the network chain conformation and deformation but also distributions in potentially inhomogeneous samples.[19,20] In this study we will extend our previous study, which focused on filler effects on the average network chain deformation[20] but lacked an in-depth theoretical analysis of the NMR data.

Earlier NMR work was mostly limited to the study of spectral splittings in deuteron (^{2}H) spectra of labeled samples.[21−30] The observation of such splittings is restricted to stretched samples, and they provide only a qualitative measure of local orientation. It has in fact been argued that the splittings are mostly due to the nonelastic defect fraction,[31] which is supported by the facts that similar splittings are also observed for low molar mass probe chains[23] and that the apparent defect fraction as detected by MQ NMR is maximal at the magic-angle orientation of stretched samples.[20] This means that the splitting characterizes the network anisotropy through diffusional averaging over a larger length scale, and it is thus not surprising that the cited studies usually confirm adherence to an affine deformation model, rendering it equivalent to the classic phenomenon of strain birefringence.[32]

^{1}H MQ NMR[11] is based upon very similar basic principles, but in-depth information on orientation correlations obtained in the unstretched state serves as a crucial reference for experiments on stretched samples. Only more recently, a new numerical approach to extract distributions of local orientations characteristic for all network chains also from ^{2}H spectra has been published[33] but has yet to be applied in systematic studies. Because of the intrinsic millisecond-scale time average, the segmental orientation is evaluated as a quasi-static plateau value of the time-dependent segmental orientation function, owing to the fact that the segmental fluctuations take place on a sub-microsecond time scale at sufficiently high temperature. The plateau value is referred as the local dynamic orientational order parameter of the polymer backbone, S_b.[34] For a given chain, the order tensor related to S_b points along the connection vector **R** between two local constraints, which may be physical cross-links and/or (trapped) entanglements. As mentioned, S_b is measured in terms of an average residual dipole−dipole coupling constant, D_{res},

$$D_{res} = D_{eff} S_b \tag{1}$$

where D_{eff} is an effective coupling constant characteristic for the Kuhn segment of the specific polymer, comprising a preaveraging due the intrasegmental motions.[35]

The microscopic length scale of the MQ experiment is defined by S_b and is directly related to the local density of constraints or cross-links. Its theoretical description is related to the classical treatment of the stress-optical rule by Kuhn and Grün;[32] S_b scales in bulk samples with the inverse average number of segments of the elastically active subchains N, providing the connection to the apparent network chain density $D_{res} \sim N^{-1} \sim M_{c,app}{}^{-1}$ and thus to the modulus. In addition, we have a relation to the squared, time-averaged end-to-end distance R^2,[36]

$$S_b \approx \frac{3}{5N}\frac{R^2}{R_0{}^2} \tag{2}$$

where $R_0{}^2$ is the constant, strain-independent squared equilibrium end-to-end distance of a subchain. If Gaussian statistics is applicable on all relevant length scales, this expression may be further simplified using $R_0{}^2 = Nb^2$, where b is the characteristic length of a statistical segment (Kuhn length). Hence, for sufficiently long chains and moderate elongations, $(S_b)^{1/2}$ and $(D_{res})^{1/2}$ scale linearly with $R = |\mathbf{R}|$ and hence with the tensile forces acting at the ends of the chain.[36] It can thus be taken to study local strain (and stress) of polymer networks.[20]

Again, we stress that **R** to be used in eq 2 is the separation between cross-linked points only for the case of highly cross-linked networks free from entanglement effects. **R** is most closely related to the length scale corresponding to the plateau of the dynamic structure factor probed in NSE experiments.[14] For lower cross-link densities, **R** is thus rather related to the tube diameter, and its change upon deformation would correspond to what is probed in a SANS experiment in the limit of short labeled paths.[15] We remind again that S_b is robustly found to be directly proportional to the macroscopic elasticity modulus,[8,12,13] which means that it probes the length scale (conformational space) relevant for entropy elasticity. Thus, predictions of simple network models for S_b are straightforward, as long as they provide an assumption or a prediction of the local deformation of **R** in eq 2. Tube models are not straightforward in this context, but one explicit treatment of S_b has been published[37] for the Heinrich−Straube tube model in the limit of weak entanglement constraints (dominating cross-links), using the continuous Gaussian chain model in combination with the Edward mean-field formalism.[38] In this description, the confining potential, m, is related to an external force which keeps fluctuating chain segments on the primitive path of an ideal chain.[37] For a weak potential ($m^2N^2b^2 \ll 1$) it was found that the individual chain segments tend to orient transversely with respect to the end-to-end vector, which leads to a reduced orientational order parameter $S_b{}^w$:[39]

$$S_b{}^w \cong \frac{3}{5N}\frac{\langle R_{HS}{}^2\rangle^w}{R_0{}^2}\left(1 - \frac{75}{4}m^2 N R_0{}^2\right) \tag{3}$$

Taking the ensemble average of the end-to-end distance $\langle R_{HS}{}^2\rangle^w/R_0{}^2 = 1 + m^2N^2b^2/3$, the relation may be further reduced to $S_b{}^w \cong (3/5N) - 11m^2R_0{}^2$.[37] In contrast to the treated case of weak constraints, strongly confined (entanglement-dominated) chain segments tend to orient with the tube and perform sliding motions *along* the tube,[40] and it is hypothesized that a relation may exist to the extremely long mechanical relaxation times of lowly cross-linked, entangled, and defect-rich networks.[41,42] Our current study is thus restricted to moderately and well cross-linked networks. Nevertheless, in order to confront our data with predictions of different other entanglement theories of rubber elasticity, we will tentatively take **R** to scale with the predicted deformation dependence of the tube diameter.

In the present paper we will use MQ NMR experiments performed on natural rubber (NR) samples stretched *in situ*

dx.doi.org/10.1021/ma5012655 | Macromolecules 2014, 47, 7597−7611

and numerical calculations to discuss the local strain distributions in networks with different cross-link densities. We demonstrate the capability of the NMR experiments to reveal independent information on distributions of local chain stretching and their orientations, which enables a detailed comparison between experiments and available network models. We also review NMR results published for other polymer networks and demonstrate them to be in qualitative agreement with our more detailed observations.

II. NETWORK MODELS

Uniaxial deformation of an elastomer along the axis z can be defined by the elongation ratio $\lambda^{mac} = z'/z$ and is described by the three-dimensional elongation matrix expressing incompressibility of the material, Λ_{mac} (subscript "mac" stands for "macroscopic"), with

$$\Lambda_{mac} = \begin{pmatrix} \lambda_{mac}^{-1/2} & 0 & 0 \\ 0 & \lambda_{mac}^{-1/2} & 0 \\ 0 & 0 & \lambda_{mac} \end{pmatrix} \quad (4)$$

where $\lambda_{mac}^{-1/2}$ and λ_{mac} are the eigenvalues for the axes perpendicular and parallel to z, respectively.

Theoretical network models attempt to relate the elastic response of the networks chains (local deformation) to the macroscopic deformation. Currently, the main descriptions are the affine fixed-junction model (AM),[43] the phantom model (PM),[44] the Rubinstein/Panyukov,[45] and the Heinrich/Straube[46] tube models (TM), in which the tube deformation is anisotropic but subaffine, and finally the molecular stress function model (MSFM) of Wagner,[5] which implements the special case of an isotropic tube model.

The AM rests on the assumption that the fluctuations of the network junctions are completely suppressed by strong interactions with neighboring chains[43] and describes the microscopic network deformation as the relocation of the (fixed) network junctions according to the macroscopic deformation matrix of eq 4. Segmental fluctuations and reorientations are allowed.[32] Consequently, we find $\mathbf{R}$ to be affinely transformed and the local deformation, $\lambda_{loc,\alpha} = R_\alpha/R_0$ (α = ||, $\perp$), in directions parallel and perpendicular to the stretching direction to relate directly to the macroscopic elongation, λ_{mac}:

$$\lambda_{loc,\parallel}^{AM} = \lambda_{mac}$$
$$\lambda_{loc,\perp}^{AM} = \lambda_{mac}^{-1/2} \quad (5)$$

The AM leads to a highly elongated deformation ellipsoid of the set $\{\mathbf{R}_i\}$ of all end-to-end vectors (Figure 1A). The affine prediction was found to disagree with early experimental findings from SANS, e.g., refs 1, 47, and 50. Still, the junction affine model has so far been the only model used to explain NMR results of strained elastomers.[22,27,51−53] A reason for this might be the (apparent) agreement of the spectral line shape predictions of unstrained polymer networks with the affine Gaussian chain model. Below we also present a more extended analysis of literature spectra, which accounts also for nonelastic defects, and discuss the deviations from the AM.

As an alternative, the PM derived by James and Guth[44] allows the network junctions to fluctuate around their mean positions. A further assumption of the PM is the strain

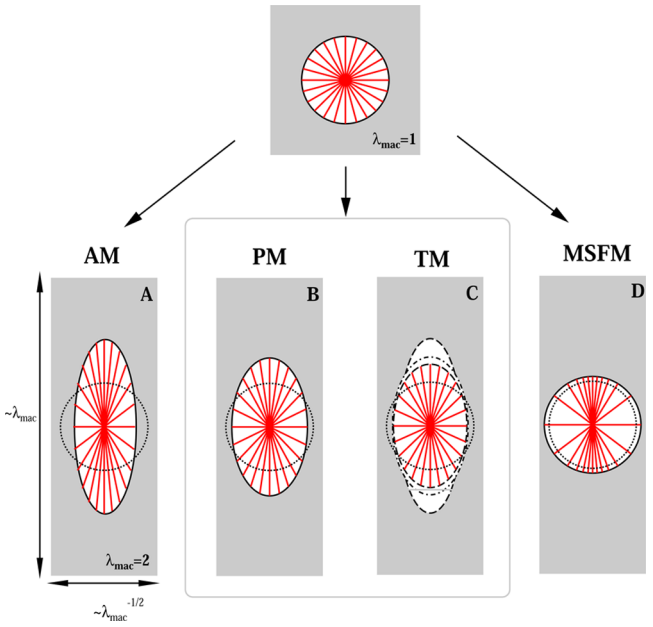

Figure 1. Model predictions of lengths and orientations of the end-to-end vectors in an undeformed and uniaxially deformed networks using the junction-affine model (A), the phantom model (B), the tube model (C), and the molecular stress function model (D). The gray areas depict the change of the macroscopic dimensions upon uniaxial deformation. In C the dashed ellipsoids indicate the deformations above and below the affine length scale, and the dash-dotted line is the prediction of the Mergell−Everaers double tube model in the limit of large deformations.

independence of the fluctuation potential, while the transformation of the average junction positions is affine. This approach results in a reduced local deformation as depicted in Figure 1B. The local deformation of a tetrafunctional network can be described by

$$\lambda_{loc,\parallel}^{PM} = \left(\frac{1 + \lambda_{mac}^{2}}{2}\right)^{1/2}$$
$$\lambda_{loc,\perp}^{PM} = \left(\frac{1 + \lambda_{mac}}{2\lambda_{mac}}\right)^{1/2} \quad (6)$$

which represents a specific implementation of the PM that was derived by using the model description derived for SANS experiments[10] and eq 2 of ref 5. It should be noted that λ^{loc} does not describe the ensemble average only, but also the time average of single chain conformations.

Since the PM does not account for topological constraints (besides the possible implementation of interchain interactions into the fluctuation potential[54]), numerous tube models have been developed in which the chains are confined by neighboring chains in a tube-like region.

As a direct consequence of the PM, the first TM derived by Warner and Edwards assumes a deformation-independent tube diameter.[55] Later, Heinrich and Straube[46] as well as Rubinstein and Panyukov[45] derived nonaffine TMs, which both take the tube diameter to deform proportionally to the square root of the affine deformation. This nonaffine description was successfully proven to fit mechanical[56] as well as NSE data[14] of uniaxially strained, highly entangled polymer networks. However, mechanical measurements under biaxial deformation

dx.doi.org/10.1021/ma5012655 | Macromolecules 2014, 47, 7597−7611

cannot be fully explained by these TMs,[6] and recent simulations indicate an even weaker dependency of the local deformation on the macroscopic strain.[57]

In relation to our analyses, chain dimensions above an affine length scale of $R_{aff} = bN_e^{1/2}\lambda_\alpha^{3/2}$, which was derived by Rubinstein and Panyukov,[45] are supposed to scale affinely with the macroscopic deformation, while below R_{aff} chain conformations are only "very little" affected and supposed to scale as the tube diameter:[7]

$$\lambda_{loc,\parallel}^{TM} = \begin{cases} \lambda_{mac} & \text{for } R > R_{aff} \\ \lambda_{mac}^{1/2} & \text{for } R < R_{aff} \end{cases} \quad (7)$$

$$\lambda_{loc,\perp}^{TM} = \begin{cases} \lambda_{mac}^{-1/2} & \text{for } R > R_{aff} \\ \lambda_{mac}^{-1/4} & \text{for } R < R_{aff} \end{cases} \quad (8)$$

These relations are visualized by the two dashed ellipsoids in Figure 1C. Since the lateral dimension of uniaxially deformed networks is always reduced, the case $R > R_{aff}$ for the lateral dimension is not considered in the figure. For networks that are not dominated by entanglements, Mergell and Everaers developed a "double tube" model by combining the TMs of Rubinstein−Panyukov/Heinrich−Straube and of Warner−Edwards,[58] the latter providing phantom limiting behavior for the case of dominating cross-links. In the limit of large extensions ($\lambda_{mac} > 3$) they found that the entanglement contribution generally vanishes in the stretching direction, and the deformation becomes phantom-like (see dashed-dotted line in Figure 1C). Perpendicular to the stretching direction the entanglements always dominate the local properties, resulting in a tube-like behavior.

In contrast to these TMs, Boué et al.[59] proposed a description of lowly cross-linked networks in which only the chain orientations, but not |**R**| is changed upon macroscopic deformation. Modifying this approach by including a tube-induced local deformation under applied strain which is still assumed to be isotropic, Wagner derived the MSFM,[5] which describes the response of a network on the microscopic (SANS) as well as on the macroscopic scale (Mooney stresses) surprisingly well. Finally, in comparison to the previously discussed network model, the MSFM shows the least pronounced local effective deformation following

$$\lambda_{loc,\parallel/\perp}^{MSFM} = \frac{1}{2}\lambda\left(1 + \frac{\sinh^{-1}\sqrt{\lambda_{mac}^3 - 1}}{\sqrt{\lambda_{mac}^3}\sqrt{\lambda_{mac}^3 - 1}}\right) \quad (9)$$

as is depicted in Figure 1D.

III. MATERIALS AND METHODS

A. Samples. In this study we investigated two series of vulcanized *cis*-1,4-polyisoprene (natural rubber, NR) samples; for details on the preparation we refer to refs 13 and 20. The samples from series A (NR1A,NR3A1, NR3A2) and series B (NR1B, NR3B) are made from Standard Malaysian Rubber SMR5L and SMRCV60, respectively. The average molecular weight of the network chains between two cross-links, M_c, can be estimated by the relation $M_c^{-1} = M_{c,app}^{-1} - M_e^{-1}$ using the experimental apparent molecular weight $M_{c,app}$ and the critical value for entanglement dominated networks M_e known from the literature, assuming a constant entanglement contribution.[8] For all samples M_c was found to be in between 1100 and 2100 g/mol, which is well below the critical value for entanglement dominated networks of ∼6200 g/mol.[8,60] $M_{c,app}$ was determined by MQ NMR experiments (see below), using the relation[11,18,35]

$$M_{c,app} = \frac{617\ \text{Hz}}{\bar{D}_{res}/2\pi}\frac{\gamma - 2}{\gamma}\ \text{kg/mol} \quad (10)$$

The functionality γ of the cross-links is set to 4, as NR chains have a high molecular weight between 100 000 and 1 000 000 g/mol. Samples NR1A, NR3A1, and NR3A2 are identical to samples 1, 3a, and 3b, respectively, of ref 13 where the perfectly linear, semiquantitative correlation of the NMR-based $M_{c,app}^{-1}$ to its mechanically determined modulus-based counterpart was proven. Also, a (of course qualitative) Mooney−Rivlin analysis was further applied to demonstrate the importance of entanglement contributions[8] to the nonlinear stress−strain behavior of these samples.[13] It is stressed that sulfur-vulcanized NR belongs, in our hands, to the most homogeneous and defect-poor elastomers available[17,19] and that strain-induced crystallization is not expected to play a significant role (see below).

B. Uniaxial Deformation. The experimental assessment of the strain response of the rubber samples was realized by two different methods leading to the same deformation matrix, as depicted in Figure 2:

(1) Following our previous work,[20] die-cut sets of rubber rings of variable inner (d_i) and outer (d_a) diameters were elongated and stripped onto a thin ceramics blade (width w = 9.5 mm, thickness e = 0.64 mm, l being defined as $l = 2(w + e)$). The final elongation was varied by using different combinations of inner and outer diameters (d_i = 1.5−3 mm, d_a = 3−5 mm) while keeping the ring widths constant (Δd = 1.5 mm). The weighted average of the stretching parameter λ_{mac} was calculated by

$$\lambda_{mac} = \frac{l}{\pi}\frac{1/d_i - 1/d_a}{\ln(d_a/d_i)} \quad (11)$$

and is further used as a parameter to characterize the degree of deformation.

(2) Pieces of rubber of 1 mm thickness and variable sizes were uniaxially stretched to a prescribed uniaxial elongation λ_{mac} (measured from the distance between two marks on the sample) with a homemade device and simultaneously sandwiched between Teflon sheets and fitted into two carved pieces of Teflon which were screwed together, maintaining all three dimensions of the stretched sample at the required values.

In both deformation methods 1 and 2, the sample holder was stepwise rotated around its axis using a computer-controlled servo motor (MSR 0020/L2-45-0, Mattke AG, Freiburg, Germany) to vary the angle Ω between the elongation axis and the magnetic field, as schematically shown in Figure 2. The angular accuracy was about 1°.

C. Low-Field MQ NMR Experiments. The experiments were conducted on two different mq20 Bruker minispec low-field NMR spectrometers operating at 0.5 T with $\pi/2$ pulses of 2.6 and 1.95 μs length and dead times of 11 and 15 μs, respectively. Comparative experiments showed an overall good agreement of the two systems and ensured the reproducibility of our findings. All experiments were conducted at temperatures between 70 and 90 °C ($T_g \sim -60$ °C), allowing to remove not only initial but also strain-induced crystalline components. The individual temperatures (depending on the sample

Table 1. Comparison of the Average D_{res}, Corresponding Apparent Molecular Weights ($M_{c,app}$), and Defect Volume Fractions of Samples Investigated in This Study (Values Correspond to the Results without Uniaxial Deformation)

sample	$D_{res}/2\pi$ (Hz)	$M_{c,app}$ (g/mol)	defects (%)
NR1A	158	1950	12.3
NR1B	148	2100	10.6
NR3A1	280	1100	6.0
NR3A2	271	1150	5.5
NR3B	260	1200	4.1

dx.doi.org/10.1021/ma5012655 | Macromolecules 2014, 47, 7597−7611

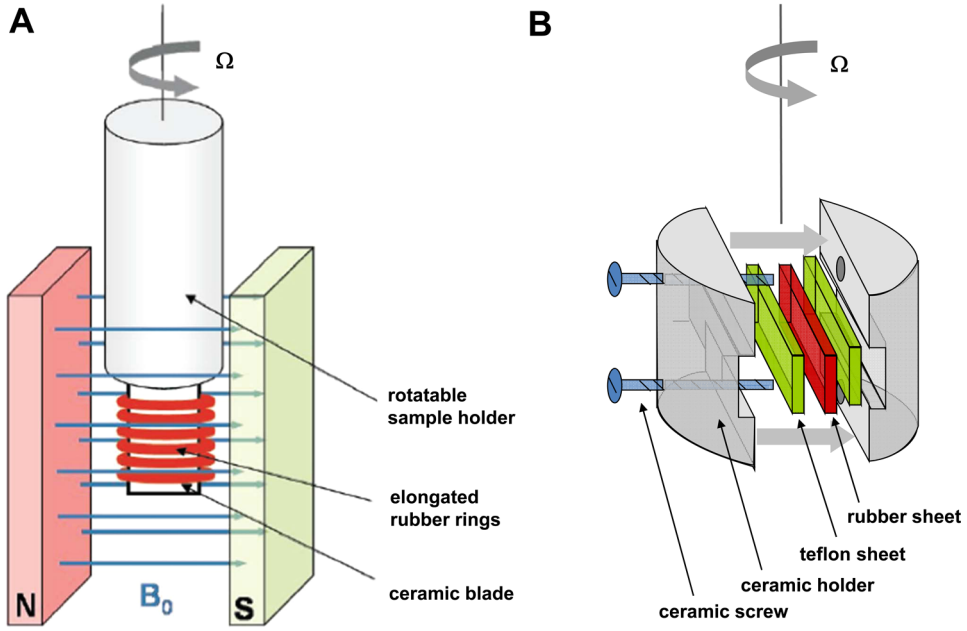

Figure 2. Deformation of the rubber samples was realized either by elongation of rubber rings (A) or by replacing the ceramic blade by a ceramic holder for pre-stretched samples (B). Orientation-dependent measurements were conducted by rotation of the sample holder.

and the applied strain) were determined by the onset of crystallization found in control experiments.

A detailed description of the MQ experiment and the analysis of the raw signal functions can be found in our previous publications[11,19,20] and in the Supporting Information (SI1). We just note here that the central analyzed quantity is the normalized double-quantum (DQ) intensity buildup as a function of a DQ pulse sequence time τ_{DQ}

$$I_{nDQ}(\tau_{DQ}) = \langle \sin^2(D_{res,i} P_2(\cos\theta_i)\tau_{DQ})\rangle_i \quad (12)$$

where $D_{res,i} = (3D_{eff}/5N)(R_i^2/R_0^2)$ (see eqs 1 and 2). The ensemble average $\langle ... \rangle_i$ extends mainly over all different possible chain orientations but may also include an additional apparent $D_{res} \sim N^{-1}R^2/R_0^2$ distribution characterizing sample inhomogeneities. We stress again that all R values represent time averages $\langle R^2\rangle_t^{1/2}$ over the usual instantaneous Gaussian R distribution. The angle θ describes the time-averaged orientation of a segment, which is parallel to **R**, with respect to the magnetic field. The determination of the distribution function of effective dipole−dipole coupling constants D_{res} from the experimental I_{nDQ} (rather than just fitting an average value $\bar{D}_{res}$) is an ill-posed problem but can be realized by regularization methods. We applied a method which was specifically designed and tested on model-inhomogeneous polymer networks, being based on an experimentally derived kernel function.[19] This approach has the advantage that not only the initial part of the normalized buildup curve but all points up to its plateau value of 0.5 are fitted, enabling access to a broad range of dipolar interactions and revealing possible inhomogeneities, as reflected by broad or even multimodal distributions.

As a robust alternative, theoretical considerations[61] show that the MQ raw signal functions can also be suitably combined to yield a dipolar-dephasing function that is equivalent to the result of a Hahn echo experiment. In this way, the dipolar second moment $\sim\bar{D}_{res}^2$ can be obtained from a fit to such data, or dipolar spectra can be obtained by Fourier transformation, and integrated to obtain the same second moment. This allows for a completely model-independent check of the main result of the regularization analysis, as demonstrated below. For details, we refer to the SI1B in the Supporting Information.

D. Numerical Calculations. We performed numerical calculations in which the network response was calculated by sampling over a sufficiently large set of randomly distributed end-to-end vectors, stretched, and possibly reoriented as described by the different deformation laws (see Figure 1). The initial length distribution was chosen to be either described by a δ function or an alternative probability function derived from experimental data (see below). The routine is described in more detail in SI2 of the Supporting Information.

IV. RESULTS

A. Average Local Deformation of Network Strands. *Experimental Results of Uniaxially Deformed NR.* Any orientational effect of the dipolar interaction was removed from the data by sampling over a set of sample orientation angles Ω_j (see Figure 2) and constructing an "artifical powder" by summing the normalized DQ buildup curves:[20]

$$I_{nDQ}^{powder} = \sum_j I_{nDQ}(\Omega_j)\sin\Omega_j \quad (13)$$

This approach enables the application of previously developed procedures[19] to retrieve the local stress distributions in isotropic samples also in the stretched networks.[20] The dipolar interaction involves the time-averaged orientation of a segment, which is along R_i and thus expressed as a function of the angle between R_i and the magnetic field. It can then be expressed as a function of Ω and of the angle between R_i and the stretching direction α_i (see Figure 5) through standard composition of angular functions.[20]

The deformation was realized by controlled stretching of either rubber rings or rubber sheets, as described in the Materials and Methods section. Figure 3 demonstrates the comparability of both approaches, as the obtained normalized DQ buildup curves as well as the derived D_{res} distributions are in good agreement for NR samples of similar cross-link densities. The applied macroscopic strain results in an overall shift to higher residual couplings (Figure 3), an increased distribution width σ reflecting an apparently enhanced inhomogeneity, and a tail appearing at high D_{res} values corresponding to the most highly stressed polymer chains. The only difference between the two experimental approaches was the slightly higher homogeneity obtained by stretching of sheets, as indicated by a somewhat reduced relative width of the distribution ($\sigma/\bar{D}_{res}$ = 0.44 instead of 0.49).

dx.doi.org/10.1021/ma5012655 | Macromolecules 2014, 47, 7597−7611

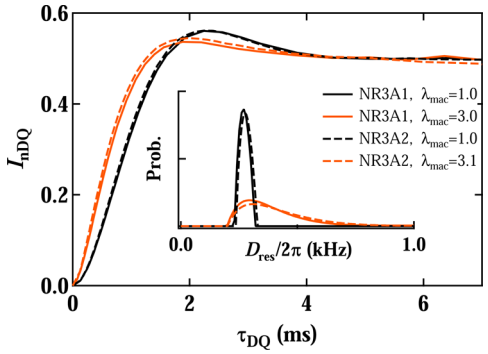

Figure 3. DQ buildup curves of unstretched (black) and stretched (orange) NR of similar cross-link densities obtained by stretching of rubber rings (NR3A1, $\bar{D}_{res,\lambda_{mac}=1}/2\pi$ = 280 Hz, λ_{mac} = 3.0, line) or sheets (NR3A2, $\bar{D}_{res,\lambda_{mac}=1}/2\pi$ = 271 Hz, λ_{mac} = 3.1, dashed). The respective D_{res} distributions (inset) confirm the good agreement of the two experimental approaches. The slight shift of the curves originates from the slightly different cross-link densities.

The average value $\bar{D}_{res}$ can be determined by either taking the weighted average of the distributions derived from time-dependent DQ buildup curves (Figure 4A) or, alternatively, from the respective dipolar spectra (Figure 4B) or their time-domain counterparts, which can be calculated from the MQ data (see Supporting Information SI 1B for details). Note that the apparent doublet in the spectra is *not* an effect of orientation (as it is also present in the unstretched sample), but rather arises from the particular shape of DQ buildup curves and is due to multiple-quantum spin dynamics.[62]

While the full D_{res} distribution allows for the calculation of the first as well as the second moment, initial-rise fits to time domain data ($I_{nDQ} \propto \overline{D_{res}^2}\tau_{DQ}^2$) necessarily yield a second moment. From the spectra, a first moment can also be obtained by half-sided integration, which is correct in the limit of vanishing homogeneous line broadening. All methods show nearly the same dependence upon elongation (Figure 4C), which proves that our central results are not subject to uncertainties related to the numerical regularization analysis of the nDQ buildup curves. Only the second moment from the distributions deviates somewhat, but we note that this quantity is particularly vulnerable to numerical inaccuracies (weak tails toward higher D_{res}). We therefore focus in the following on the first moments.

Comparison with Model Predictions. The change of the time-averaged length of a chain between two local constraints with an end-to-end vector of length R_0 at an angle α_i with respect to the direction of the applied force can be described by (see Figure 5)

$$R'_i{}^2/R_0{}^2 = \lambda_{loc,\perp}{}^2 + (\lambda_{loc,\parallel}{}^2 - \lambda_{loc,\perp}{}^2)\cos^2\alpha_i \qquad (14)$$

and is directly related to $D_{res,i}$ of that chain (eqs 1 and 2). $\lambda_{loc,\parallel}$ and $\lambda_{loc,\perp}$ are the model-dependent *local* deformation ratios parallel or perpendicular to the direction of the force (see section II).

The angle of the end-to-end vector with respect to the direction of the force decreases from α_i to α_i' (Figure 5) with increasing macroscopic deformation according to the relation

$$\tan\alpha_i' = (\lambda_{loc,\perp}/\lambda_{loc,\parallel})\tan\alpha_i \qquad (15)$$

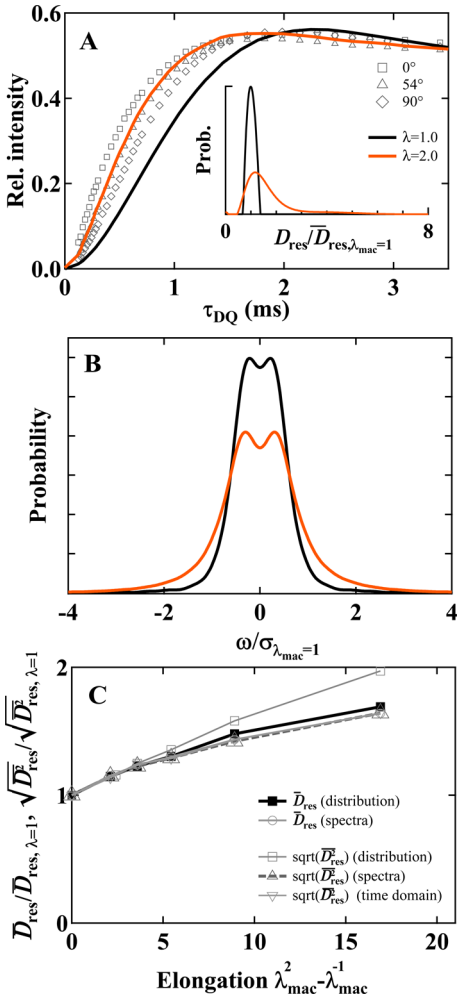

Figure 4. DQ buildup curves (A), D_{res} distributions (A, inset), and dipolar spectra (B) of NR1B at λ_{mac} = 1.0 (black) and λ_{mac} = 2.0 (orange). The symbols in A show the result for different orientations of the sample with respect to the magnetic field: 0° (squares), 54° (rhombs), and 90° (triangles); the lines in A and B represent the calculated "artificial powder" average. The determination of $\bar{D}_{res}(\lambda)$ is largely independent of the method (C): average relative values from D_{res} distributions (squares) as well as determined by initial-rise analysis or from spectra.

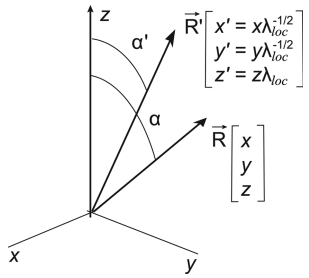

Figure 5. Deformation of the end-to-end vector of a network (sub)chain upon stretching along the z direction.

which describes a rotation of the end-to-end vector toward the direction of the applied force. By averaging over all orientations j, the average local deformation can be written as

$$\frac{\bar{D}_{res}(\lambda_{mac})}{\bar{D}_{res,\lambda_{mac}=1}} = \frac{\langle R^2\rangle_j}{R_0{}^2} = \frac{1}{3}(\lambda_{loc,\parallel}{}^2 + 2\lambda_{loc,\perp}{}^2) \qquad (16)$$

dx.doi.org/10.1021/ma5012655 | *Macromolecules* 2014, 47, 7597−7611

Importantly, it is thus shown that the *ensemble average* does not depend on an initial apparent R or R_0 distribution, which is related to the D_{res} distribution (with average $\bar{D}_{res}$) of an inhomogeneous network chain ensemble (see the next section for details).

Combining eq 16 with the network model descriptions of eqs 5−9, the experimentally derived local deformation of the NR samples can be compared with predictions of the network models (see Figure 6). While the AM and the PM are usually considered to represent the upper and the lower limit for real networks, respectively, we found the data for $\lambda_{mac} \geq 1.5$ to be below the PM prediction. Previous implementations of the phantom model assumed that restrictions due to mutual segmental interactions as well as network deformation can be appropriately considered by constrained junction fluctuations.[54,63] These approaches lead, however, to a deformation dependence of the relative $\bar{D}_{res}$ which is below the AM but always above the PM prediction. Hence, the deviation of our results from the PM to lower values at higher stains is an indication that the transmitted stress or strain cannot be projected onto the junction fluctuation potential alone but is also transferred by the confinement of surrounding network chains (i.e., a tube).

As explained in the Introduction, the influence of a weak tube constraint onto the chain motional anisotropy can be modeled by the Edwards tube (ET) mean-field approach.[37] Combining eqs 3 and 16, we find $\bar{D}_{res}(\lambda)$ to be determined by

$$\frac{\bar{D}_{res}(\lambda_{mac})}{\bar{D}_{res,\lambda_{mac}=1}} = \frac{1}{3}[(1 - Cm_{\perp}^{2})\lambda_{loc,\parallel}^{2} + 2(1 - Cm_{\parallel}^{2})\lambda_{loc,\perp}^{2}] \tag{17}$$

with $C = 75R_0^2N/4$. Equation 17 can be now used in combination with the AM as proposed by Sommer et al.[37] or any other network model. To fit eq 17 to the data set, we assumed the λ dependence of the confining potential m to behave as the tube diameter in the TM, as both originate from excluded volume effects of the network matrix. Hence, we used $m_{\perp}^2 = m_{\lambda=1}^2/\lambda_{mac}^{-1/2}$ and $m_{\parallel}^2 = m_{\lambda=1}^2/\lambda_{mac}$. However, the AM could not be fitted without violating the condition $m^2N^2b^2 \ll 1$ under which eq 17 holds. Using the PM description of eq 6 instead, reasonable agreement of the experimental data could be obtained using $Cm_{\lambda=1}^2 = 0.375$ (see the dashed line in Figure 6).

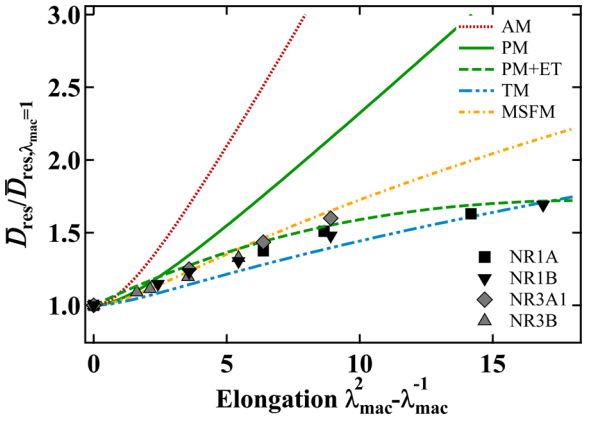

Figure 6. Relative increase of $\bar{D}_{res}$ with elongation of NR networks (symbols) in comparison with the various models (lines): junction affine model (AM, red dotted), phantom model (PM, green solid), the tube model (TM, blue dot-dot-dashed), and the molecular stress function model (MSFM, yellow dot-dashed). The best agreement is given by the a combination of the phantom model and a weak confining potential of the Edwards tube mean-field description (PM +ET, green dashed).

B. Apparent End-To-End Distance Distributions. NR networks have narrow D_{res} distributions in the unstretched state[31] and broadened distributions upon deformation when the artificial powder average is considered (Figures 3 and 4). As is obvious from eq 12, the distribution of $D_{res} \sim N^{-1}R^2/R_0^2$ in the unstretched state can be related to a distribution of any of the relevant variables N, R^2, or R_0^2 ($= Nb^2$). As this distribution must be related to structural inhomogeneities on a length scale larger than the mesh size,[17,31] it is most likely related to N values that vary across the sample. However, the presence of regions with nonequilibrium R values, as fixed by topological constraints (trapped entanglements), can also be envisioned. Since all variables are coupled, we take on a practical approach and simply map the $D_{res} \sim R^2$ distribution onto what we call an *apparent R^2 distribution*. This wording is mainly motivated by mathematical convenience, as the necessary distribution integrals correspond to simple convolutions in any case. We note that the origin of the observed, surprisingly narrow apparent R^2 distributions found in unstretched networks is as yet unclear and the subject of ongoing work.[36,64] Local force-balance effects[36] as well as the fact that NMR measures a time-averaged quantity that extends beyond the level of a subchain with fixed R_0 may play a role.

It is quite intuitive that distributions under stretch should be broader than in the relaxed state because end-to-end vectors with different orientations are transformed differently, as depicted schematically in Figure 1. In the following we implement these schematic deformation patterns and compare the experimental findings for the apparent R^2 distributions with the corresponding model predictions.

Upon stretching, a vector R of squared length R^2 is deformed into R' as schematized in Figure 5 and given by eq 14. In the unstretched, isotropic state, the angular density of end-to-end vectors is $\sin\alpha\, d\alpha$. In the stretched state, the distribution $Q_{\lambda_{loc}}(R')$ of end-to-end vector lengths corresponding to an isotropic ensemble of end-to-end vectors of length R_0 in the unstretched state is given by

$$Q_{\lambda_{loc},R^2}(R'^2)\, dR'^2 = \sin\alpha\, d\alpha \tag{18}$$

Differentiating eq 14

$$dR'^2 = -2R_0^2(\lambda_{loc,\parallel}^2 - \lambda_{loc,\perp}^2)\sin\alpha\cos\alpha\, d\alpha \tag{19}$$

and using, from eq 14

$$\cos\alpha = \left(\frac{\frac{R'^2}{R_0^2} - \lambda_{loc,\perp}^2}{\lambda_{loc,\parallel}^2 - \lambda_{loc,\perp}^2}\right)^{1/2} \tag{20}$$

in which the ratio $\lambda_{loc,\parallel}^2 \leq R_\lambda^2/R_0^2 \leq \lambda_{loc,\perp}^2$, we obtain

$$Q_{\lambda_{loc},R^2}(R'^2) = \frac{1}{2(\lambda_{loc,\parallel}^2 - \lambda_{loc,\perp}^2)^{1/2}(R'^2 - \lambda_{loc,\perp}^2R_0^2)^{1/2}} \tag{21}$$

Again, $\lambda_\parallel$ and $\lambda_\perp$ describe the model specific local deformations along the parallel and perpendicular axes.

For a length distribution $P(R^2)$ or equivalently $P(D_{res})$ in the relaxed state, assuming that each member of the R^2 distribution

dx.doi.org/10.1021/ma5012655 | Macromolecules 2014, 47, 7597−7611

behaves independently of the others, the expected R' distributions $Q_{\lambda_{loc}}(R')$ can then be computed as the integral

$$Q_{\lambda_{loc}}(R'^2) = \int_0^\infty P(R^2) Q_{\lambda_{loc},R^2}(R'^2)\, dR^2 \quad (22)$$

where $Q_{\lambda_{loc},R^2}(R'^2)$ is given by eq 21. Figure 7 shows the model predictions for the distributions $Q_{\lambda_{loc},R^2}(R'^2)$ for a single (time-averaged) value R^2 of the initial squared end-to-end vector (panel A) in comparison with $Q_{\lambda_{loc},R^2}(R'^2)$ of the rubber sample NR1B (panel B).

The plots illustrate that the elongated sample exhibits a narrower D_{res} distribution as compared to the AM, PM, and even TM predictions, even though the initial apparent R^2 distribution of the NR sample is broader than a δ distribution. The broadening effect due to the convolution is, however, seen to be weak, so thanks to the homogeneity of the samples, our analyses do not depend significantly on the independence assumption mentioned above. According to eq 22, a broad initial distribution should always lead to an even broader distribution under stress if the models were applicable. Since similar results of rather narrow distributions under stretch are consistently found for all investigated NR samples, the conclusion drawn from the increase of the average $\bar{D}_{res}$ upon elongation (Figure 6) is again confirmed: the effective microscopic elongation is rather weak as compared to most network model predictions.

In order to elucidate possible origins of this behavior, the effects of strain on the apparent end-to-end distance distribution and/or the chain orientation can be investigated separately, benefiting from their experimental separation made possible by the "artificial powder average". Thus, the next section discusses the orientation effects.

C. Chain Orientations. For the determination of $\bar{D}_{res}$ and the D_{res} distributions, powder-averaged DQ intensities were used to cancel out orientation effects on the measured dipolar interactions. In this section the anisotropic feature of the DQ intensities is specifically addressed to obtain information regarding the chain orientations. Without orientational averaging, the contribution of a single chain to $I_{nDQ}(\tau_{DQ})$ does depend not only on the absolute value of R_i but also on its mean orientation θ_i with respect to the magnetic field (see eq 12).

Accordingly, polymer chains parallel to the stretching direction ($\alpha_i = 0$, therefore $\theta_i = \Omega$) are expected to show no contribution to I_{nDQ} if the sample is oriented with the stretching direction at the magic angle $\Omega_{MA} = 54.7°$ with respect to the magnetic field (such that $P_2(\cos\theta_i) = 0$). For an elongated network, the contributions of chains with deviant orientations (see Figure 1) reduce this strong angular dependency and only a minimum at finite values of I_{nDQ} is expected to develop close to Ω_{MA}, which serves as a measure for the local anisotropy and should become more apparent if the applied strain increases.

To verify the local strain induced orientation in a polymer network, the orientation-dependent DQ intensity should be first compared directly with the models discussed earlier.

The DQ intensity at a constant short τ_{DQ} in the initial-rise region (which is representative of $\bar{D}_{res}$) obtained with the sample NR1B for each sample orientation, normalized by its powder-averaged value, is plotted in Figure 8 as a function of the angle Ω. Experimental results are compared with the model predictions of the orientation-dependent DQ intensity, as obtained from numerical calculations using again the initial D_{res} distribution of the NR sample. The comparison shows that the overall applicability of the models is rather limited, as none of the models describe the experimental finding very well. A better agreement can only be achieved if the orientation of the chains is further reduced, as it is possible with a variant of the MSFM (dashed curve in Figure 8).

To obtain this result, we combined the isotropic deformation obtained in the MSFM (eq 9) with different chain orientation distributions, as schematized in Figure 9. Figure 9A depicts the

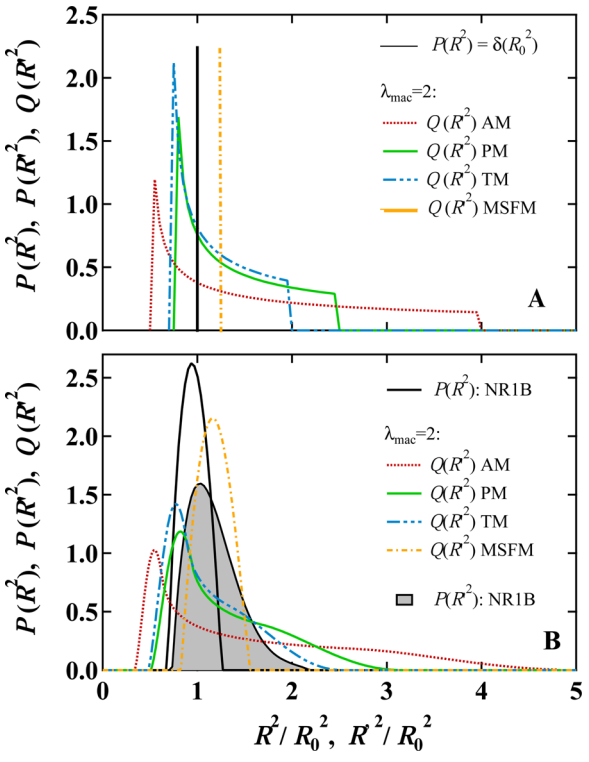

Figure 7. D_{res} distributions ($\sim R^2$) predicted by the various models for a delta distribution $P(R) = \delta(R - R_0)$ (A) and for an experimentally determined distribution of NR1B using eqs 21 and 22 (B).

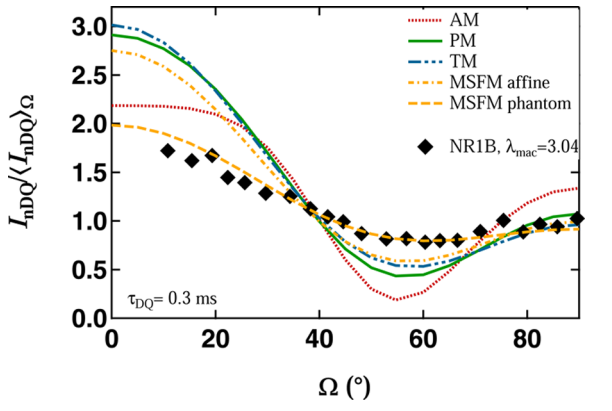

Figure 8. Relative normalized DQ intensities at a constant DQ evolution time for different sample orientations Ω with respect to the magnetic field together with model predictions. The experimental data represent NR1B at the macroscopic deformation of $\lambda_{mac} = 3$ and $\tau_{DQ} = 0.3$ ms.

dx.doi.org/10.1021/ma5012655 | Macromolecules 2014, 47, 7597−7611

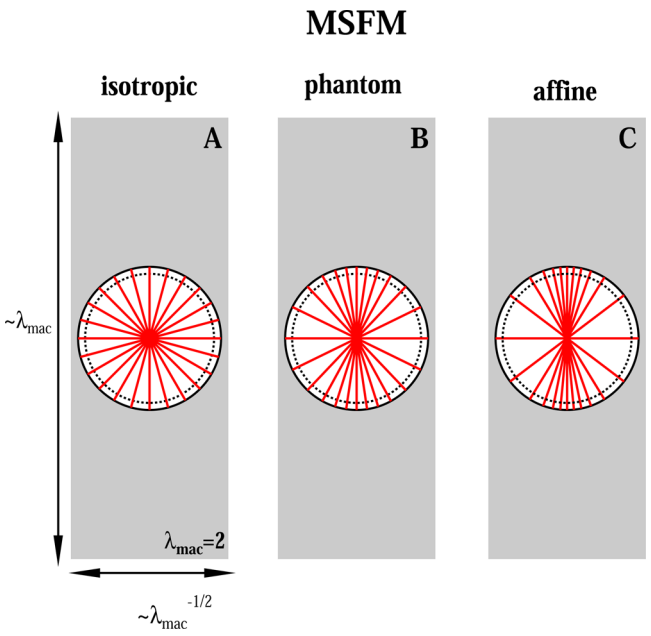

Figure 9. Local chain orientations for the molecular stress function model of an isotropic network (A) and in combination with the contracted phantom (B) and contracted affine (C) deformation models.

MSFM without any preferred chain orientations upon stretching (a clearly unrealistic model), and Figure 9C visualizes the affine MSFM as introduced by Wagner.[5] The latter model assumes the same chain orientation distribution as predicted by the AM and is called the "affine rotation model"[5] or the "contracted affine model".[59] Interestingly, Boué and co-workers[59] have also discussed a "contracted phantom model", which predicts a weaker strain-induced orientation. A combination of the MSFM approach of Wagner with the contracted phantom model of Boué exhibiting a less pronounced orientation anisotropy (Figure 9B) reflects the experimental data best (dashed line in Figure 8).

We note that we are currently not able to implement predictions of the Edwards-tube weak-constraint approach for the actual D_{res} distributions as well as the orientation effects (rather than modeling them both on the basis of apparent R^2 distributions). This is due to a lack of educated assumptions on the relation of the angle-dependent transformation properties of the $\lambda_{loc,i}$ and m_i^2 in eq 17 and their possible coupling. However, the structure of eq 17 suggests that an additional weak tube constraint (which lowers local order parameter values and thus distribution and orientation effects), which transforms in a specific way, may well be able to explain all our data.

As an alternative, inspired by the approach of Boué and co-workers to separate orientation and deformation of the end-to-end vectors, we developed a new approach to extract apparent orientation distributions directly from the experimental data with numerical calculations of oriented network chains. Assuming an isotropic chain distribution in the unstretched network, the anisotropy of the chain orientation distribution in the stretched state can be characterized by the single parameter, $\kappa = \lambda_\perp^\ddagger/\lambda_\parallel^\ddagger$, with $0 \le \kappa \le 1$ according to eq 15. We use this parameter to compare the experimental data with the model descriptions of eqs 5−9.

It should be emphasized that κ does not change the length of R, but only the orientations of individual chains. As there is no unique relation between changes in length and in orientation of network chains upon stretching (this depends on the microscopic model), we may vary independently these quantities in order to reproduce both the D_{res} distributions obtained from powder spectra (Figure 7) and the angular variation (Figure 8) for various degrees of stretching. We have chosen a direct correlation between R and the chain orientation, assuming that highly deformed chains are closer to the z-axis than less deformed ones. The intensity anisotropy was thus simply fitted to the experimental data by iteratively adjusting κ; for details see SI2B of the Supporting Information. Note that the position of the minimum can deviate from the exact value of $\Omega = 54.7°$ due to contributions from network chains at different orientations relative to each other. Figure 10 shows the results for NR1B and NR1A at $\lambda_{mac} = 2.0$ and $\lambda_{mac} = 3.8$, respectively. The fitted orientation distributions of the chain lengths are depicted in the insets and can be qualitatively compared with Figure 1.

The results of a quantitative analysis of all samples at all elongations are shown in Figure 11. In panel A the orientation parameter κ is shown for the different samples as well as for the network models. In a nutshell, these data represent strong evidence that the strain-induced local chain orientations are much less pronounced than predicted. The same aspect is shown in panel B where the apparent chain length deformations along the main axes are plotted. The experimental values of $\lambda_\perp^{loc}$ and $\lambda_\parallel^{loc}$ were directly extracted from the dimensions of the deformation ellipsoid of the numerical fits (see insets in Figure 10). Surprisingly, the chains parallel to the deformation behave similar to the PM, although neither the average deformation (Figure 6) nor the distributions (Figure 7) could be well described by the PM. Perpendicular to the stretching axis nearly no deformation is indicated, which means

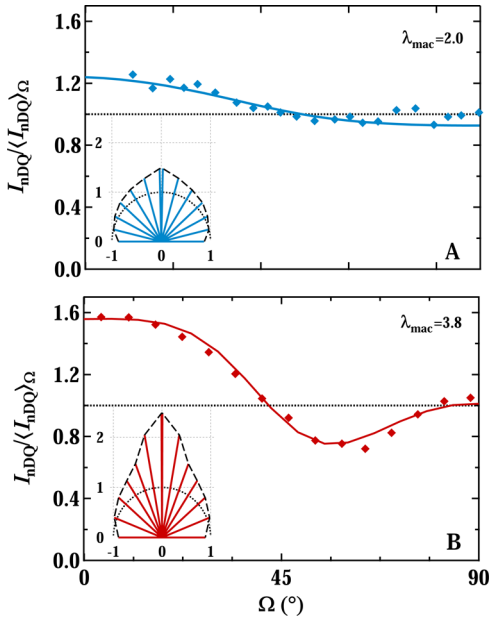

Figure 10. Relative DQ intensities (symbols) of NR1B at $\lambda_{mac} = 2.0$ (A) and NR1A at $\lambda_{mac} = 3.8$ (B) together with the numerical fits (lines). The insets depict the respective local chain orientations and display the experimentally determined R distributions and can be directly compared to the model predictions of Figure 1.

dx.doi.org/10.1021/ma5012655 | Macromolecules 2014, 47, 7597−7611

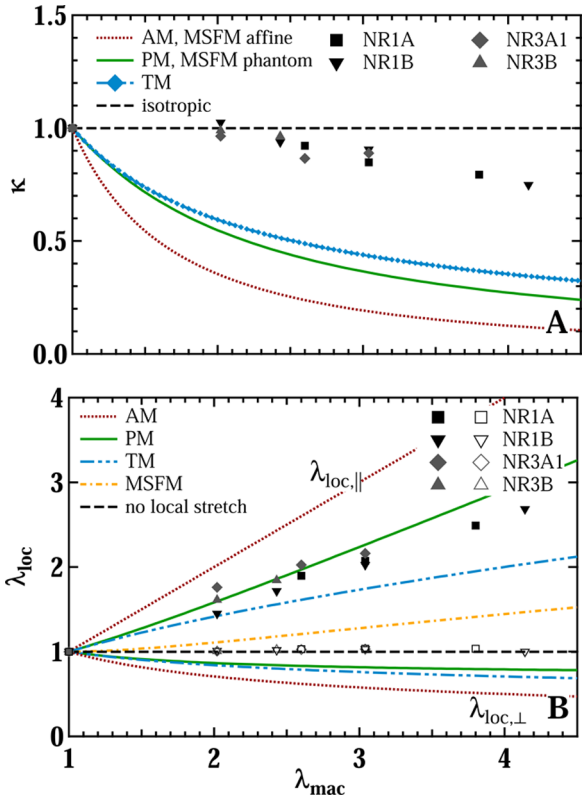

Figure 11. Chain orientation parameter κ (A) and local deformations in parallel and perpendicular to the applied strain (B) of all investigated NR networks together with model predictions.

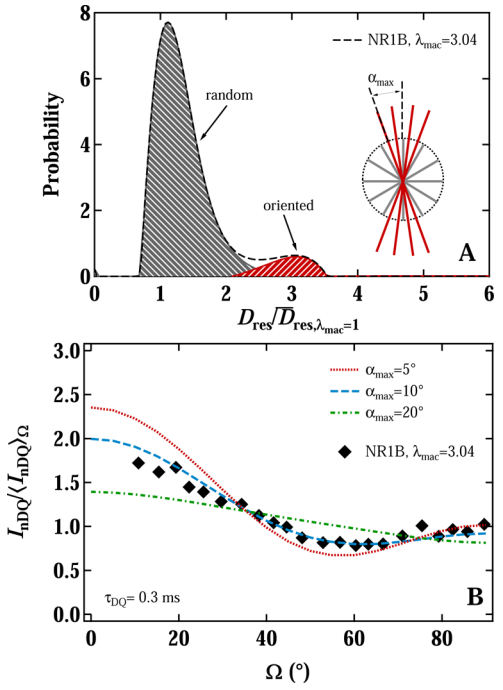

Figure 12. D_{res} distribution of NR1B (A) shows indications of two maxima, which can be referred to a less strained, randomly oriented (black) and a highly oriented and strained (red) fraction. The comparison with the intensity anisotropy (B) shows the best agreement if the highly oriented strains are also strongly oriented, with $\alpha_{max} \leq 10°$.

that the reasons for the powder-average data to be below the PM prediction (see Figure 6) are the overall weak orientation and the strong deviation of the deformation geometry from an ellipsoid. This can be inferred from a comparison of Figures 1 and 10 and leads to an implicit reduction of $\bar{D}_{res}$ that is stronger than predicted by eq 16. The surprising compliance with the PM along the z direction is in fact reminiscent of the large-strain prediction ($\lambda > 3$) of the double tube model[58] (see the Network Models section).

Highly deformed network samples (Figure 12A) show a rather pronounced heterogeneity in the D_{res} distribution, as indicated the presence of a separate maximum at higher D_{res}, corresponding to a small population of highly strained chains. Thus, we finally tested a bimodal situation, by assuming that chains with a high D_{res} value are more likely to be strongly oriented, while chains with a low D_{res} are assigned to less deformed network regions in which the chains stay isotropically oriented (inset). Using such a description, we obtain, e.g., for NR1B at $\lambda_{mac} = 3.04$ a local deformation of $\bar{D}_{res}/\bar{D}_{res,\lambda=1} \approx 1.2$ for the isotropically oriented chains (gray fraction) and $\bar{D}_{res}/\bar{D}_{res,\lambda=1} \approx 3.3$ for the oriented chains (red fraction), which correspond to about 10% of the total number of segments. In this situation, the intensity anisotropy depends only on the orientations of the highly stressed chains, while the isotropically oriented chains do not contribute to the intensity anisotropy (Figure 12B). Numerical calculations of the intensity anisotropy by using the average final deformations of Figure 12A and a narrow initial length distribution gave a reasonable agreement with the experimental data if the strained chains have an orientation of $\alpha < 10°$, where α is the angle between the chain orientation and the axis of deformation (inset in Figure 12A).

V. DISCUSSION

We have shown that, by analyzing separately the D_{res} distributions and the angular variation of the normalized DQ signals obtained by MQ NMR, information on both the chain elongation and orientation can be extracted from these experiments performed on elastomer samples stretched in situ, giving a complete picture of the local strain at a microscopic scale. Our main result is that the average local strain found in our stretched NR samples is significantly below the PM prediction. An analysis based upon separating the strain effect on the length of the end-to-end vectors and their orientation revealed that only the rather small fraction of network chains parallel to the strain follows the PM, while the transverse direction as well as the orientations are hardly affected. We remind again that NMR generally measures the average chain deformation and (re)orientation on a very local scale (see eq 2 and the related discussion in the Introduction).

In contrast to the AM, the PM allows junction fluctuations but neglects any topological constraints. Modifications of the PM include additional local constraints by changing the fluctuation amplitude of the cross-links and its deformation under macroscopic strain, e.g., the intermediate model of Ronca and Allegra[54] or variations of the AM of Flory, Erman, and co-workers.[63,65,66] All of these models project all possible interactions with neighboring chains on a fluctuation ellipsoid of the network junctions. While such an approach is not unrealistic, as real networks show reduced fluctuations compared to predictions of the PM,[67] the average local strain of the NR samples (Figure 6) is already below the PM

dx.doi.org/10.1021/ma5012655 | Macromolecules 2014, 47, 7597−7611

prediction at elongations above $\lambda_{mac} \geq 1.5$, in contrast to any of these models.

Before we continue our discussion of possible explanations, we turn to checking whether the large body of published NMR data is compatible with our findings, mainly in order to confirm that our observations are of general, sample-independent nature. This is mainly to demonstrate that there is no inconsistency with the previous NMR data *per se* but only with their analyses. These mostly focus on (often weak) spectral splittings that vanish at zero deformation, that are likely dominated by the nonelastic defect fraction,[31] that are certainly a many-chain effect, and, importantly, that trivially reflect affine behavior due to a diffusional average (see below). We thus seek to review published data from ^{2}H NMR experiments and to compare them with the present results of ^{1}H MQ NMR. In principle, ^{2}H NMR probes the same type of information as it also reflects a time-averaged interaction tensor, in this special case the quadrupolar coupling tensor, which is in the static limit parallel to the C–^{2}H bond in the labeled moiety. For a comparison, we need to evaluate the overall changes in shape and width of the published ^{2}H spectra upon stretching in relation to the relaxed state, extract a suitable measure, and compare it with a similar quantity from the MQ data. We are further required to focus on measurements at a specific orientation (usually $\Omega = 0°$ or 90°, i.e., stretching parallel or perpendicular to B_0).

The extraction of suitably square-averaged apparent D_{res} values (second moments) from DQ buildup curves or spectra is in fact uncritical, as shown in Figure 4B and the SI 1B (Supporting Information), and these analyses can be done also for single orientations rather than artificial powders. On the other hand, the ^{2}H spectra have a complex shape with often ill-defined baseline, so for a reliable analysis we tentatively decompose them into an elastic and an apparent defect contribution.

There is strong experimental evidence that defect-poor networks show a Gaussian shape,[31] which is at a first glance in contrast to the "super-Lorentzian" line shape observed in many ^{2}H NMR experiments, e.g., refs 22, 23, and 27. As such a line shape naturally results from the Gaussian chain model, it has been widely taken as an evidence for the applicability of the Gaussian chain model to describe polymer networks. Opposing this rather common interpretation, we mention the strong deviations from the Gaussian model evidenced by early SANS measurements[1,47−50] and the fact that NMR measures a time-averaged quantity and does not likely reflect a quasi-static Gaussian end-to-end distribution of R.

This apparent contradiction can be resolved by simply interpreting the super-Lorentzian line as a composite shape made up of a broad Gaussian-like network response and a narrow defect contribution at the center frequency. Importantly, this interpretation does not need additional theoretical assumptions that explain the origin of the strain-induced splitting.[22,23,27] Clearly, it arises from the nonisotropic averaging of the tensorial interactions of rather mobile material (mostly dangling structures) embedded in an anisotropic network matrix. Such a diffusional average may well extend over larger scales beyond the affine length scale of Rubinstein/Panyukov,[45] explaining that the splitting follows the affine stress-optical law.[32]

Usually, "nematic interactions" on segmental orientations are invoked to explain the presence and the magnitude of the splitting, and these have also been claimed to possibly contribute to the overall elasticity.[68−70] Yet, we note that the splitting is usually rather small as compared to the full width of the spectra, so even though being prominent, its contribution to the integral observable is not large, as shown below. It should be mentioned that spectra for stretched PDMS model networks made of long ($M > M_e$) precursors have been reported,[53] in which also the network component appears to show a splitting. This contradicts the general interpretation and clearly deserves further studies, but again, the fact that nematic interactions may be more relevant for long and entangled chains in special cases does not mean that they exert a dominating influence at high cross-linking.

Thus, a tentative line shape analysis by spectral decomposition enables us to describe the spectra in terms of separate network and apparent defects responses and perform a comparison with our data. We reanalyzed published experimental data for PDMS[23,53] and PB networks,[22,27] and refer to the SI3 of the Supporting Information for details. Each individual spectrum was fitted by a superposition of one (or two) Lorentzian(s), which we relate to the apparent defect response of the relaxed (or stretched) polymer, and a network component, which was either approximated by a single Gaussian or by a combination of a Lorentzian and a Gaussian. Figures 13A and 13B show exemplarily the extracted network contributions of PB[22] and PDMS[51] samples, respectively, that form the unsplit broad base of the spectra, while the split apparent defect contributions have a consistent amplitude at all

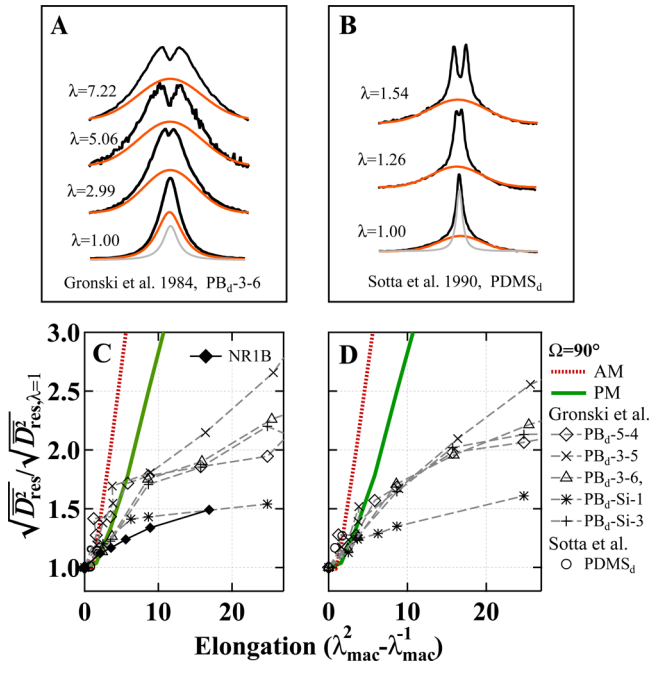

Figure 13. Extracted network components (orange lines) from ^{2}H spectra of 90°-orientated (A) PB and (B) PDMS networks published by Gronski et al.[22] and Sotta et al.,[51] respectively. The gray dashed lines represent the apparent defect fractions of the unstretched polymer networks. Panels C and D show the relative increase of local strain ($\sqrt{\overline{D_{res}}^2} \sim \sqrt{\overline{R^4}}$) versus macroscopic elongation $\lambda_{mac}^2 - \lambda_{mac}^{-1}$, retrieved from the same works as compared to our results from ^{1}H MQ NMR. The apparent defect contributions are included and excluded in panels C and D, respectively. The thick lines are corresponding theory predictions (which deviate from those of the powder-averaged first moment, eq 16).

dx.doi.org/10.1021/ma5012655 | *Macromolecules* 2014, 47, 7597−7611

λ. More detailed plots can be found in SI3 of the Supporting Information.

An estimate of the second moment $\sim\overline{D_{res}^2}$ of either the full spectrum or the network contributions only can then be obtained from a fit $\sim \exp\{-k\overline{D_{res}^2}t^2\}$ to the initial decay region (first 10%) of the time-domain representation of the best-fit results after inverse Fourier transformation. Its square root is directly related to the average residual quadrupolar interaction. The ratio of the latter to the unstretched reference is equivalent to $\sqrt{\overline{D_{res}^2}}/\sqrt{\overline{D_{res,\lambda=1}^2}}$, so we are able to directly compare the literature results with MQ data for the same sample orientation of $\Omega = 90°$ (Figure SI 5E shows a corresponding plot for the few available data for 0° of Ries et al.[27]). Importantly, we remind that in MQ NMR the defects can only be separated at the magic-angle orientation,[20] while they are part of the dipolar-coupled fraction at other angles, in particular at the canonical orientations. We therefore compare our data with literature data including (Figure 13C) and excluding (Figure 13D) the apparent defect-related component.

For both cases, we consistently observe a similar increase of the relative average interaction strengths with macroscopic elongation, which is for all networks at high elongations well below the AM and PM predictions. Note that the ^{2}H data include both peroxide-vulcanized (fully and junction-labeled) as well as end-linked model systems. The nondominant contribution of the spectral splitting is thus demonstrated. The literature data clusters above the trend observed for our samples, but we remind that we can extract only a second-moment-related quantity from the former, which is more susceptible to baseline inaccuracies and sample inhomogeneities. It is noted that in the work of Gronski et al.[22] a full line shape analysis was indeed performed, and a comparison with the unstretched state was made (arriving at the conclusion that the AM apparently works well up to extensions of $\lambda_{mac} \approx 2$). Yet, the interpretation was rooted in the assumptions that no residual quadrupolar interaction is present in the unstretched state and that local constraints to anisotropic segmental motion (as in our work represented by the length of R) are not strain-dependent. This is disproven by all MQ NMR experiments on unstretched networks (revealing a finite $\bar{D}_{res}$ and a perfect correlation with the elasticity) and is also unrealistic, opposing the picture conveyed in Figure 1.

Therefore, coming back to the main point of the discussion, the deviations from the affine and phantom models observed for our data as well as the literature data are an indication that even for samples with rather short network chains, tube-like confinement effects of the surrounding matrix cannot be ignored. Any alternative model, modifying the junction fluctuations, would only predict behaviors in-between the AM and the PM. Indeed, local packing effects as identified in dry networks can lead to enhancements of the local D_{res}, which may even change with applied strain, as recently found in swelling experiments.[71]

The TM, originally developed for entangled polymers,[72] implements excluded-volume effects and was successfully proven to describe uniaxially strained polymers of high molecular weight.[56] Surprisingly, at high elongations the TM seems to become a more reasonable approach also for the cross-link-dominated polymer networks studied herein, and it can be argued that at high extensions not only the fluctuations of the network junctions but also the lateral conformational space of the chains is reduced by neighboring chains. This assumption was verified by fitting our data of the average $\bar{D}_{res}$ to the ET model for the order parameter developed by Sommer et al.[37] This mean-field approach is an excellent tool to study the onset of excluded-volume interactions of polymer network chains. As a result, we found that the addition of a weak confining potential allows to describe the experiments even if a phantom-like deformation of the cross-link positions is assumed.

Maybe the picture of an entanglement-free polymer network should be questioned altogether, in view of the growing indications that entanglements play a role even for highly cross-linked samples. As to mechanical properties, it is well-known that the affine and phantom models predict the same neo-Hookean stress−strain response.[73] However, deviations from this prediction, which are clearly apparent in a nonzero Mooney−Rivlin C_2 parameter, are not only observed for our investigated samples[13] but are the rule rather than the exception even in highly cross-linked samples (see ref 8 for a detailed discussion). In this reference, we have demonstrated that the tube-based entanglement theories considered herein, which all predict subphantom deformation (see Figure 1), can straightforwardly explain such a behavior. Attempts to quantitatively correlate results from different macroscopic methods such as mechanical and swelling experiments,[13,74] and also including microscopic information from, e.g., NMR[8] or wide-angle X-ray scattering,[13] point in the same direction. Results from SANS[15] focusing on short labeled paths suggest phantom-like behavior, but were only performed for moderate deformation ($\lambda < 2$), and are further subject to uncertainties related to defects.[9] In turn, recent NSE data[14] are in accord with tube-model predictions. Finally, abundant theory work exists as well; for instance, MD simulations showed that the elastic modulus of a relaxed polymer network could be well described neither by the AM nor by the PM.[75] In summary, our finding of subphantom deformation behavior appears to be in line with various results from the literature.

In spite of the confining effects of the surrounding network matrix, the average anisotropy of the local deformation is not enhanced and even below all model predictions (Figures 8 and 11). As discussed already, the deviations may be due to our currently incomplete understanding of tube-constraint effects on the actual distributions of the apparent local order ($\sim D_{res}$) and the orientation effects. We are hoping for more theoretical support in order to further develop our work in this direction, focusing of course also on a wider variety of samples, such as end-linked model systems and entanglement-dominated networks. As an alternative to such tube-model-based efforts, network rearrangements on the mesoscopic scale,[76] caused by e.g. an inhomogeneous distribution of tensile forces as indicated by the apparent length distribution profiles with a tail at high D_{res} values (Figure 12), may play a role. As our analysis suggests that such high-D_{res} tails may correspond highly stressed as well as oriented polymer chains, this interpretation supports the idea that most of the forces are transmitted by a few network chains. This was in fact derived earlier from analyses of MC simulations of swollen and stretched networks.[77]

VI. CONCLUSIONS

We were able to analyze the average chain deformation, the apparent chain length distributions, and their average orientation in moderately to highly cross-linked natural rubber upon uniaxial elongation, using a modern ^{1}H NMR technique

dx.doi.org/10.1021/ma5012655 | Macromolecules 2014, 47, 7597−7611

and relying on a data analysis procedure based upon intentional averaging over experiments performed at different sample orientations in the magnet. A comprehensive comparison of the experimental results with predictions of the affine fixed-junction model, the phantom model, and different tube model variants showed that in spite of the large value range of the model predictions, none of the models was suitable to describe all the different measured local properties.

As a support of the new technique, the average network deformations of our rubber samples were compared and found to be rather similar to what can be derived from other NMR results for variety of polymer networks taken from the literature, independently of their individual chemical composition and molecular weight, which indicates that rather universal aspects are addressed in our study. At the core of this comparison is the reanalysis of published NMR spectra, separating the pure network response from apparent defect contributions and analyzing the effective width of these spectra as a function of strain with and without the consideration of the apparent defect fraction. The literature results are thus consistently demonstrated to be in line with our observations, further demonstrating that the potential defect fraction does not exert a large influence on the observed overall microscopic deformation.

The deviations from the network model predictions, namely the narrow apparent chain deformation distributions and the low orientational order upon strain, could be rationalized by local tube-induced confinement effects or semilocal rearrangements leading to an inhomogeneous force transmission through a minority fraction of highly stretched and oriented chains. Clearly yet, not only the network junctions transmit the applied strain or stress but also the neighboring chains influence the local configurational space of the network chains by excluded-volume interactions.

Thus, we finally advertise the recent theoretical work of Sussmann and Schweizer,[78] who present an alternative interpretation of entangled rubber elasticity in terms of intermolecular packing constraints of primitive-path segments instead of entropic arguments related to longitudinal chain stretching along the tube. These new ideas are in tune with earlier suggestions stressing the importance of potential nematic interactions on segmental orientations in networks, as mentioned above.[68−70] These could well have a contribution to the overall elasticity and are most apparently reflected in the residual orientations observed for nonelastic defect fractions. The consequence of such new physics on the molecular observables investigated herein and, on our quantitative understanding of the mechanical properties of elastomers in general, has yet to be evaluated.

■ ASSOCIATED CONTENT

Supporting Information

^{1}H NMR spectroscopy details, numerical calculations, and lineshape decomposition of ^{2}H NMR spectra. This material is available free of charge via the Internet at http://pubs.acs.org.

■ AUTHOR INFORMATION

Corresponding Authors

*E-mail maria.ott@physik.uni-halle.de (M.O.).

*E-mail kay.saalwaechter@physik.uni-halle.de (K.S.).

Notes

The authors declare no competing financial interest.

■ ACKNOWLEDGMENTS

The authors thank Jens-Uwe Sommer for insightful discussions and his valuable comments on the manuscript. Funding was provided by the DFG-ANR German-French joint project "DINaFil", SA982/6-1.

■ REFERENCES

(1) Beltzung, M.; Picot, C.; Herz, J. Investigation of the chain conformation in uniaxially stretched poly(dimethylsiloxane) networks by small-angle neutron scattering. *Macromolecules* **1984**, *17*, 663−669.

(2) Ullman, R. Small-angle neutron scattering from elastomeric networks. Application to labeled chains containing several crosslinks. *Macromolecules* **1982**, *15*, 1395−1402.

(3) Gottlieb, M.; Gaylord, R. J. Experimental Tests of Entanglement Models of Rubber Elasticity. 1. Uniaxial Extension. *Polymer* **1983**, *24*, 1644−1646.

(4) Gottlieb, M.; Gaylord, R. J. Experimental Tests of Entanglement Models of Rubber Elasticity. 3. Biaxial Deformations. *Macromolecules* **1987**, *20*, 130−138.

(5) Wagner, M. H. Analysis of Small-Angle Neutron Scattering Data on Poly(dimethylsiloxane) Network Unfolding. *Macromolecules* **1994**, *27*, 5223−5226.

(6) Urayama, K.; Kawamura, T.; Kohjiya, S. Multiaxial Deformations of End-linked Poly(dimethylsiloxane) Networks. 2. Experimental Tests of Molecular Entanglement Models of Rubber Elasticity. *Macromolecules* **2001**, *34*, 8261−8269.

(7) Rubinstein, M.; Panyukov, S. Elasticity of Polymer Networks. *Macromolecules* **2002**, *35*, 6670−6686.

(8) Schlögl, S.; Trutschel, M.-L.; Chassé, W.; Riess, G.; Saalwächter, K. Entanglement Effects in Elastomers: Macroscopic vs Microscopic Properties. *Macromolecules* **2014**, *47*, 2759−2773.

(9) Read, D. J.; McLeish, T. C. B. "Lozenge" Contour Plots in Scattering from Polymer Networks. *Phys. Rev. Lett.* **1997**, *87*, 87−90.

(10) Pearson, D. S. Scattered Intensity from a Chain in a Rubber Network. *Macromolecules* **1977**, *10*, 696−701.

(11) Saalwächter, K. Proton multiple-quantum NMR for the study of chain dynamics and structural constraints in polymeric soft materials. *Prog. Nucl. Magn. Reson. Spectrosc.* **2007**, *51*, 1−35.

(12) Cohen-Addad, J. P.; Thanh, B. P.; Montes, H. Evidence for a Linear NMR-Elasticity Interrelationship in Polymeric Gels. *Macromolecules* **1997**, *30*, 4374−4380.

(13) Vieyres, A.; Pérez-Aparicio, R.; Albouy, P.-A.; Sanseau, O.; Saalwächter, K.; Long, D. R.; Sotta, P. Sulfur-cured Natural Rubber Elastomer Networks: Correlating Crosslink Density, Chain Orientation and Mechanical Response by Combined Techniques. *Macromolecules* **2013**, *45*, 889−899.

(14) Pyckhout-Hintzen, W.; Westermann, S.; Wischnewski, A.; Monkenbusch, M.; Richter, D.; Straube, E.; Farago, B.; Lindner, P. Direct Observation of Nonaffine Tube Deformation in Strained Polymer Networks. *Phys. Rev. Lett.* **2013**, *110*, 196002.

(15) Westermann, S.; Pyckhout-Hintzen, W.; Richter, D.; Straube, E.; Egelhaaf, S.; May, R. On the Length Scale Dependence of Microscopic Strain by SANS. *Macromolecules* **2001**, *34*, 2186−2194.

(16) Gilra, N.; Cohen, C.; Panagiotopoulos, A. Z. A Monte Carlo study of the structural properties of end-linked polymer networks. *J. Chem. Phys.* **2000**, *112*, 6910−6916.

(17) Valentín, J. L.; Posadas, P.; Fernández-Torres, A.; Malmierca, M. A.; González, L.; Chassé, W.; Saalwächter, K. Inhomogeneities and Chain Dynamics in Diene Rubbers Vulcanized with Different Cure Systems. *Macromolecules* **2010**, *43*, 4210−4222.

(18) Chassé, W.; Lang, M.; Sommer, J.-U.; Saalwächter, K. Cross-Link Density Estimation of PDMS Networks with Precise Consideration of Networks Defects. *Macromolecules* **2012**, *45*, 899−912.

(19) Chassé, W.; Valentín, J. L.; Genesky, G. D.; Cohen, C.; Saalwächter, K. Precise dipolar coupling constant distribution analysis in proton multiple-quantum NMR of elastomers. *J. Chem. Phys.* **2011**, *134*, 044907.

(20) Pérez-Aparicio, R.; Schiewek, M.; Valentín, J. L.; Schneider, H.; Long, D. R.; Saphiannikova, M.; Sotta, P.; Saalwächter, K.; Ott, M. Local chain deformation and overstrain in reinforced elastomers: An nmr study. *Macromolecules* **2013**, *46*, 5549−5560.
(21) Deloche, B.; Samulski, E. T. Short-range nematic-like orientational order in strained elastomers: a deuterium magnetic resonance study. *Macromolecules* **1981**, *14*, 575−581.
(22) Gronski, W.; Stadler, R.; Maldaner Jacobi, M. Evidence of Nonaffine and Inhomogeneous Deformation of Network Chains in Strained Rubber-Elastic Networks by Deuterium Magnetic Resonance. *Macromolecules* **1984**, *17*, 741−748.
(23) Sotta, P.; Deloche, J.; B; Herz; Lapp, A.; Durand, D.; Rabadeux, J. C. Evidence for short-range orientational couplings between chain segments in strained rubbers: a deuterium magnetic resonance investigation. *Macromolecules* **1987**, *20*, 2769−2774.
(24) Dubault, A.; Deloche, B.; Herz, J. Effects of trapped entanglements on the chain ordering in strained rubbers: a deuterium magnetic resonance investigation. *Macromolecules* **1987**, *20*, 2096−2099.
(25) Chapellier, B.; Deloche, B.; Oeser, R. Segmental order in uniaxially strained bimodal polymer networks: a deuterium-NMR study. *J. Phys. II* **1993**, *3*, 1619−1631.
(26) McLoughlin, K.; Szeto, C.; Duncan, T. M.; Cohen, C. End-Linked Poly(dimethylsiloxane) Elastomer Structure: ^{2}H-NMR Transverse Dephasing Data Compared to Predictions of Statistical and Thermodynamic Models. *Macromolecules* **1996**, *29*, 5475−5483.
(27) Ries, M. E.; Brereton, M. G.; Klein, P. G.; Ward, I. M.; Ekanayake, P.; Menge, H.; Schneider, H. Contributions to the Total Orientation of Deformed Elastomers Arising from the Network Structure and Chain Interactions As Measured by NMR. *Macromolecules* **1999**, *32*, 4961−4968.
(28) Hedden, R. C.; McCaskey, E.; Cohen, C.; Duncan, T. M. Effects of Molecular Structure on Segment Orientation in Siloxane Elastomers. 1. NMR Measurements from Compressed Samples. *Macromolecules* **2001**, *34*, 3285−3293.
(29) Callaghan, P. T.; Samulski, E. T. Biaxial Deformation of a Polymer Network Measured via Deuteron Quadrupolar Interactions. *Macromolecules* **2003**, *36*, 724−735.
(30) Rault, J.; Marchal, J.; Judeinstein, P.; Albouy, P. A. Stress-Induced Crystallization and Reinforcement in Filled Natural Rubbers: 2H NMR Study. *Macromolecules* **2006**, *39*, 8356−8368.
(31) Saalwächter, K.; Sommer, J.-U. NMR Reveals Non-Distributed and Uniform Character of Network Chain Dynamics. *Macromol. Rapid Commun.* **2007**, *28*, 1455−1465.
(32) Kuhn, W.; Grün, F. Beziehungen zwischen elastischen Konstanten und Dehnungsdoppelbrechung hochelastischer Stoffe. *Kolloid-Z.* **1942**, *101*, 248−271.
(33) Aguilera-Mercado, B. M.; Cohen, C.; Escobedo, F. A. Extraction of Segment Orientation Distributions in Polymer Networks by Inversion of ^{2}H NMR Spectra though the Maximum-Entropy Method. *Macromolecules* **2009**, *42*, 8889−8898.
(34) Sommer, J.-U.; Saalwächter, K. Segmental order in end-linked polymer networks: A Monte Carlo study. *Eur. Phys. J. E* **2005**, *18*, 167−182.
(35) Saalwächter, K.; Herrero, B.; López-Manchado, M. A. Chain order and crosslink density of elastomers as investigated by proton multiple-quantum NMR. *Macromolecules* **2005**, *38*, 9650−9660.
(36) Sommer, J.-U.; Chassé, W.; Valentín, J. L.; Saalwächter, K. Effect of excluded volume on segmental orientation correlations in polymer chains. *Phys. Rev. E* **2008**, *78*, 051803.
(37) Sommer, J.-U.; Heinrich, G.; Straube, E. Theoretical investigation of the segment-segment correlation in topological constrained networks. *Colloid Polym. Sci.* **1990**, *268*, 148−154.
(38) Edwards, S. F.; Vilgis, T. A. The tube model theory of rubber elasticity. *Rep. Prog. Phys.* **1988**, *51*, 243.
(39) Sommer, J.-U. Theoretische Untersuchung zur Segement-Orientierungskorrelation, Master's thesis, Technische Hochschule Merseburg, 1987.
(40) Lang, M.; Sommer, J.-U. Analysis of Entanglement Length and Segmental Order Parameter in Polymer Networks. *Phys. Rev. Lett.* **2010**, *104*, 177801.
(41) Heinrich, G.; Vilgis, T. A. Long-Time Relaxation of Polymer Networks. *Macromolecules* **1992**, *25*, 404−407.
(42) Batra, A.; Cohen, C.; Archer, L. Stress Relaxation of End-Linked Polydimethylsiloxane Elastomers with Long Pendent Chains. *Macromolecules* **2005**, *38*, 7174−7180.
(43) Wall, F. T.; Flory, P. J. Statistical Thermodynamics of Rubber Elasticity. *J. Chem. Phys.* **1951**, *19*, 1435−1439.
(44) James, H. M.; Guth, E. Theory of the Elasticity of Rubber. *J. Appl. Phys.* **1944**, *15*, 294−303.
(45) Rubinstein, M.; Panyukov, S. Nonaffine Deformation and Elasticity of Polymer Networks. *Macromolecules* **1997**, *30*, 8036−8044.
(46) Heinrich, G.; Straube, E. Rubber elasticity of polymer networks: Theories. *Adv. Polym. Sci.* **1988**, *85*, 33−87.
(47) Erman, B. Chain dimensions in deformed networks: theory and comparison with experiment. *Macromolecules* **1987**, *20*, 1917−1924.
(48) Hinkley, J. A.; Han, C. C.; Mozer, B.; Yu, H. Chain Deformations in Rubber. *Macromolecules* **1978**, *11*, 836−838.
(49) Clough, S. B.; Maconnachie, A.; Allen, G. Small-Angle Neutron Scattering from Stretched Polystyrene Networks. *Macromolecules* **1980**, *13*, 774−775.
(50) Bastide, J.; Duplessix, R.; Picot, C.; Candau, S. Small angle neutron scattering and light spectroscopy investigation of polystyrene gels under osmotic deswelling. *Macromolecules* **1984**, *17*, 83−93.
(51) Sotta, P.; Deloche, B. Uniaxiality induced in a strained poly(dimethylsiloxane) network. *Macromolecules* **1990**, *23*, 1999−2007.
(52) Cohen Addad, J. P.; Soyez, E. State of gelation of randomly crosslinked polybutadiene chains. Nuclear magnetic resonance, swelling, and elongation. *Macromolecules* **1992**, *25*, 6855−6865.
(53) Genesky, G. D.; Duncan, T. M.; Cohen, C. Effect of Precursor Molar Mass on the 2H NMR Line Shapes of End-Linked PDMS Elastomers. *Macromolecules* **2009**, *42*, 8882−8888.
(54) Ronca, G.; Allegra, G. An approach to rubber elasticity with internal constraints. *J. Chem. Phys.* **1975**, *63*, 4990−4997.
(55) Warner, M.; Edwards, S. F. Neutron scattering from strained polymer networks. *J. Phys. A: Math. Gen.* **1978**, *11*, 1649.
(56) Straube, E.; Urban, V.; Pyckhout-Hintzen, W.; Richter, D.; Glinka, C. J. Small-Angle Neutron Scattering Investigation of Topological Constraints and Tube Deformation in Networks. *Phys. Rev. Lett.* **1995**, *74*, 4464−4467.
(57) Qin, J.; So, J.; Milner, S. T. Tube diameter of stretched and compressed permanently entangled polymers. *Macromolecules* **2012**, *45*, 9816−9822.
(58) Mergell, B.; Everaers, R. Tube models for rubber-elastic systems. *Macromolecules* **2001**, *34*, 5675−5686.
(59) Boué, F.; Bastide, J.; Buzier, M.; Collette, C.; Lapp, A.; Herz, J. Dynamics of permanent and temporary networks: Small angle neutron scattering measurements and related remarks on the classical models of rubber deformation. *Prog. Colloid Polym. Sci.* **1987**, *75*, 152−170.
(60) Abdel-Goad, M.; Pyckhout-Hintzen, W.; Kahle, S.; Allgaier, J.; Richter, D.; Fetters, L. J. Rheological Properties of 1,4-Polyisoprene over a Large Molecular Weight Range. *Macromolecules* **2004**, *37*, 8135−8144.
(61) Saalwächter, K.; Heuer, A. Chain Dynamics in Elastomers as Investigated by Proton Multiple-Quantum NMR. *Macromolecules* **2006**, *39*, 3291−3303.
(62) Saalwächter, K.; Ziegler, P.; Spyckerelle, O.; Haidar, B.; Vidal, A.; Sommer, J.-U. ^{1}H multiple-quantum nuclear magnetic resonance investigations of molecular order distributions in poly(dimethylsiloxane) networks: Evidence for a linear mixing law in bimodal systems. *J. Chem. Phys.* **2003**, *119*, 3468−3482.
(63) Flory, P. J.; Erman, B. Theory of elasticity of polymer networks. 3. *Macromolecules* **1982**, *15*, 800−806.
(64) Lang, M. Monomer fluctuations and the Distribution of Residual Bond Orientations in Polymer Networks. *Macromolecules* **2013**, *46*, 9782−9797.

(65) Flory, P. J. Theory of elasticity of polymer networks. The effect of local constraints on junctions. *J. Chem. Phys.* **1977**, *66*, 5720−5729.
(66) Kloczkowski, A.; Mark, J. E.; Erman, B. A diffused-constraint theory for the elasticity of amorphous polymer networks. 1. fundamentals and stress-strain isotherms in elongation. *Macromolecules* **1995**, *28*, 5089−5096.
(67) Oeser, R.; Ewen, B.; Richter, D.; Farago, B. Dynamic fluctuations of crosslinks in a rubber: A neutron-spin-echo study. *Phys. Rev. Lett.* **1988**, *60*, 1041−1044.
(68) Jarry, J.-P.; Monnerie, L. Effects of a Nematic-Like Interaction in Rubber Elasticity Theory. *Macromolecules* **1979**, *12*, 316−320.
(69) Deloche, B.; Samulski, E. T. Rubber elasticity: a phenomenological approach including orientational correlations. *Macromolecules* **1988**, *21*, 3107−3111.
(70) Oyerokun, F. T.; Schweizer, K. S. Microscopic theory of rubber elasticity. *J. Chem. Phys.* **2004**, *120*, 9359−9370.
(71) Chassé, W.; Schlögl, S.; Riess, G.; Saalwächter, K. Inhomogeneities and local chain stretching in partially swollen networks. *Soft Matter* **2013**, *9*, 6943−6954.
(72) Heinrich, G.; Straube, E. On the strength and deformation dependence of the tube-like topological constraints of polymer networks, melts and concentrated solutions. II. Polymer melts and concentrated solutions. *Acta Polym.* **1984**, *35*, 115−119.
(73) Rubinstein, M.; Colby, R. H. *Polymer Physics*; Oxford University Press: New York, 2003.
(74) Patel, S. K.; Malone, S.; Cohen, C.; Gillmor, J. R.; Colby, R. H. Elastic Modulus and Equilibrium Swelling of Poly(dimethylsiloxane) Networks. *Macromolecules* **1992**, *25*, 5241−5251.
(75) Düring, E. R.; Kremer, K.; Grest, G. S. Relaxation of randomly cross-linked polymer melts. *Phys. Rev. Lett.* **1991**, *67*, 3531−3534.
(76) Long, D. R.; Sotta, P. Stress relaxation of large amplitudes and long timescales in soft thermoplastic and filled elastomers. *Rheol. Acta* **2007**, *46*, 1029−1044.
(77) Hölzl, T.; Trautenberg, H. L.; Göritz, D. Monte Carlo Simulations on Polymer Network Deformation. *Phys. Rev. Lett.* **1997**, *79*, 2293−2296.
(78) Sussman, D. M.; Schweizer, K. S. Entangled polymer chain melts: Orientation and deformation dependent tube confinement and interchain entanglement elasticity. *J. Chem. Phys.* **2013**, *139*, 234904.